

Exploring the Thunderstorm Predictors in Indonesia

Novvria Sagita^{1,2} and Tetsuya Takemi¹

¹Disaster Prevention Research Institute, Kyoto University, Uji, Japan

²State College of Meteorology, Climatology and Geophysics., Tangerang, Indonesia

(Manuscript received 20 September 2024, accepted 3 December 2024)

Abstract Indonesia, as a tropical region and prone to frequent thunderstorms, is faced with potential risks to both human life and infrastructure. The analysis of a dataset containing observations of thunderstorms enabled us to identify variations in the vertical air temperature profiles between days experiencing thunderstorms and those characterized by no significant weather conditions (Nosig) within the layer between 1000 and 150 hPa. Examination of the relative humidity in the middle-troposphere during the thunderstorm days exhibited elevated moist layers in compared to the Nosig days across all the investigated regions. By employing stability indices that reflect the atmospheric conditions favorable for thunderstorm development, in conjunction with gridded reanalysis data and logistic regression methodologies, we ascertained that among the numerous convective stability parameters scrutinized, precipitable water (PW), K index (KI), and relative humidity in the middle troposphere (RH_Middle) emerged as the most effective parameters in distinguishing between environmental conditions conducive to thunderstorms and those devoid of significant weather phenomena. Assessment utilizing receiver operating characteristic curves illustrated that the optimal normalized thresholds for PW, KI, and RH_Middle were 0.67, 0.86, and 0.62, respectively.

Citation: Sagita, N., and T. Takemi, 2025: Exploring the thunderstorm predictors in Indonesia. *SOLA*, **21**, 51–60, doi:10.2151/sola.2025-007.

1. Introduction

Indonesia is susceptible to a higher frequency of thunderstorm compared to tropical ocean areas (Hidayat and Ishii 1999; Ramage 1968; Virts et al. 2013; Zipser 1994). Another feature of thunderstorms in Indonesia is an increased occurrence during the El Niño phenomenon (in contrast to a reduction occurrence in thunderstorms during La Niña), characterized by more pronounced activity of deep convection with denser regions of ice phase precipitation (Hamid et al. 2001; Yuan et al. 2016). Predicting thunderstorms accurately is challenging for meteorologists, owing to the complex and highly dynamic nature of the thunderstorm activity. Most thunderstorms occur on relatively small scales and evolve rapidly, making precise predictions difficult. As a result, warnings are sometimes ineffective in providing the necessary information to protect people and property (Bachok et al. 2015).

Many previous studies have used convective available potential energy (CAPE), vertical wind shear, and other commonly used atmospheric stability parameters to diagnose global thunderstorm potential (Brooks et al. 2003; Brooks 2009; Takemi 2010; Allen et al. 2011; Davies-Jones 2015, 2022; Singh et al. 2017; Taszarek et al. 2021). However, this does not eliminate the possibility of other favorable environmental indices in other parts of the world (Allen 2018). As reported in several previous studies, the most favorable indices were found not necessarily to be CAPE (Bondyopadhyay and Mohapatra 2023; Fernando et al. 2021; Hanstrum et al. 2002; Pradhan et al. 2012; Sherburn 2018; Tian et al. 2023). Hence, identifying the appropriate atmospheric stability indices that quantify the possibility of thunderstorms in tropical regions is important.

The aim of this research is to investigate the characteristics of thunderstorms in Indonesia and assess the environmental factors using a long-term reanalysis dataset. Additionally, we aim to identify the most suitable atmospheric stability index that can distinguish between thunderstorms and no significant weather and to propose predictors of thunderstorms in Indonesia.

2. Data and methodology

Figure 1 shows the study area for mainland Indonesia, utilizing gridded data over land with a resolution of 0.25×0.25 degrees. This study analyzes atmospheric stability conditions for thunderstorm days and Nosig (no significant weather) days at each grid point, using reanalysis data from 2014 to 2022.

2.1 Thunderstorm days definitions

In order to define thunderstorm days, we use data obtained from the Earth Global Lightning Detection Network (EGLN) thunder hour dataset from 2014 to 2022 (DiGangi et al. 2022) and the daily rainfall amount dataset derived

Corresponding author: Novvria Sagita, Disaster Prevention Research Institute, Kyoto University, Gokasho, Uji, Kyoto 611-0011, Japan. E-mail: novvria.sagita.55j@st.kyoto-u.ac.jp.



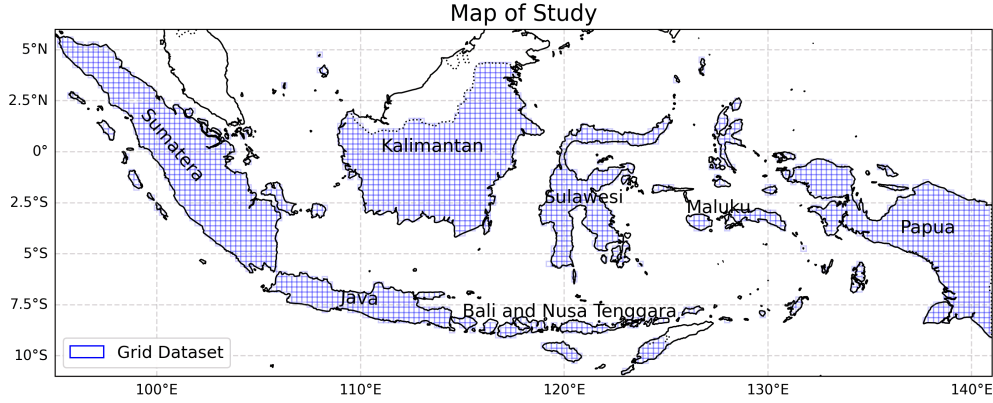


Fig. 1. Map of study.

Table 1. Stability indices and formula.

Indices	Description	Formula
SBCAPE	Surface-based convective potential energy (Hobbs and Wallace 2006)	$-R_d \int_{LFC}^{EL} (T_{v_{parcel}} - T_{v_{env}}) d \ln(p)$
RH_Middle	Average relative humidity between 700 and 400 hPa	$\frac{RH_{700} + RH_{650} + RH_{600} + \dots + RH_{400}}{8}$
SI	Showalter index (Showalter 1953)	$T_{500} - T_{p500-850}$
LI	Lifted index (Galway 1956)	$T_{500} - T_{p500}$
KI	K index (George 2014)	$(T_{850} - T_{500}) + T_{d850} - (T_{700} - T_{d700})$
TT	Total total index (Miller 1975)	$(T_{850} + T_{d850}) - (2 \cdot T_{500})$
PW	Precipitable water (Salby 1996)	$-\frac{1}{\rho g} \int_{surface}^{100hPa} r dp$
SHEAR	Shear speed between surface level to 500 hPa	$[\Delta U^2 + \Delta V^2]^{1/2}$
SWEAT	Severe weather threat index (Miller 1975)	$12[Td_{850} + 20(TT - 49) + 2(WS_{850}) + WS_{500} + 125(S + 0.2)]$
BRN	Bulk Richardson number (Markowski and Richardson 2011)	$\frac{CAPE}{0.5 \cdot (SHEAR)^2}$

from the Climate Hazards Group Infrared Precipitation with Station data (CHIRPS) spanning from 2014 to 2022 (Funk et al. 2015). Both datasets have an initial grid resolution of $0.05^\circ \times 0.05^\circ$. The daily rainfall amount data were regridded to $0.25^\circ \times 0.25^\circ$ using the bilinear interpolation method to align with the resolution of the atmospheric reanalysis dataset. On the other hand, the thunder hour data were regridded to 0.25° spacing by defining a 0.25° grid box as having a thunder hour if at least one 0.05° grid within the 0.25° box recorded thunder hour activity. Thunderstorm and no-significant weather days are defined with the use of the regridded data with the 0.25° resolution. Thunderstorm days are defined as days with at least one hour of thunder with a daily rainfall amount of 1 mm or greater from 2014 to 2022. Otherwise, we define no significant weather days (referred to as Nosig days) as having no thunder hour within the day and at the same time having a daily rainfall amount of less than 1 mm.

2.2 Atmospheric reanalysis dataset

In order to examine the atmospheric environmental conditions on days characterized by thunderstorms and Nosig days, we use the fifth-generation ECMWF reanalysis for global climate and meteorological data (ERA5) (Hersbach et al. 2020) and compute various stability index metrics (Table 1) using MetPy: A Meteorological Python Library for Data Analysis and Visualization (May et al. 2022). The indices are calculated based on the daily vertical profiles of temperature, u-component, v-component wind, and relative humidity from the ERA5 data, with the formulas displayed in Table 1.

2.3 Identifying optimal stability indices and their thresholds

To distinguish between thunderstorm and Nosig days, we used a logistic regression model. This method was chosen

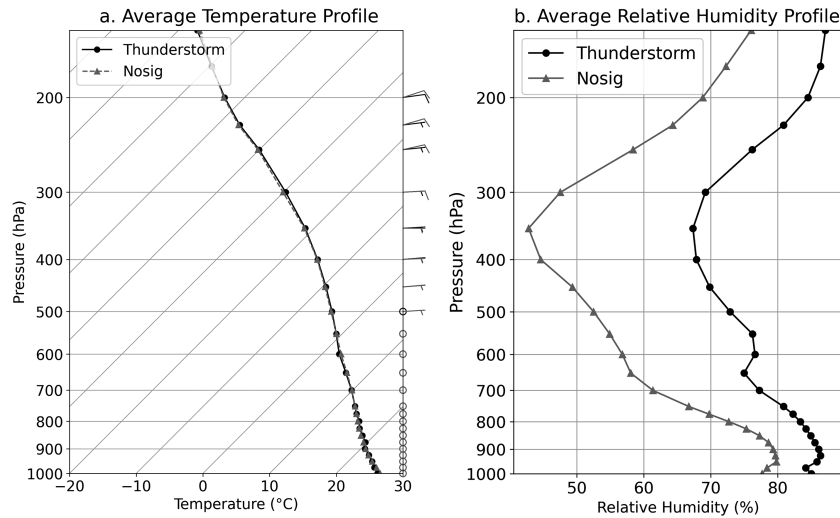


Fig. 2. The mean vertical profiles of (a) temperature (solid lines), winds (barbs), and (b) relative humidity averaged during thunderstorm days (black line) and during Nosig days (grey line).

because it is able to analyze differences in binary condition data (Salomé et al. 2020; Pang et al. 2019). First, data with RH_Middle above 100% were reset to 100% because such data are regarded as supersaturation (Hersbach et al. 2020). RH_Middle data above 100% accounted for only 0.00005% of the total data. Second, surface-based CAPE (SBCAPE) data less than 0 J/kg were also removed. To assess the environmental conditions equally by minimizing the variabilities among the locations, each stability index was normalized using MinMax Scaler, which transforms data values into a range of 0 to 1 for each grid. Then, this study constructs a logistic regression model with 60% of the normalized data as training and 40% as testing. Logistic regression was chosen because it is effective for binary classification (yes/no) and uses a probability threshold to distinguish classes (Subasi 2020) and is formulated as:

$$P(x) = \frac{1}{1 + e^{-(\beta_0 + \beta_1 x)}}, \quad (1)$$

where $P(x)$ denotes the probability of x (x refers to any parameter listed in Table 1) with a value ranging from 0 to 1, β_0 is an intercept, and β_1 is the coefficient. The optimal probability threshold is found from the receiver operating characteristic (ROC) curve by identifying the point with the maximum difference between the true positive rate (TPR) and the false positive rate (FPR) for each stability index. The optimal probability threshold was converted to an optimal normalized threshold (x) using the following formula:

$$x = \frac{\ln[P(x)/1 - P(x)] - \beta_0}{\beta_1}. \quad (2)$$

A stability index with an area under curve (AUC) exceeding 0.75 is employed to discern thunderstorm occurrences, with extraction efficacy evaluated through Probability of Detection (POD) and Probability of False Detection (POFD), where POD represents the proportion of accurately identified thunderstorm days and POFD denotes the fraction of erroneously classified days as thunderstorms. The AUC threshold of 0.75 was selected based on a previous study indicating that this value provides good accuracy for storm prediction (Swets 1988).

3. Results

3.1 The comparison of general environmental properties between thunderstorm days and Nosig days

First, we demonstrate upper-air environments on thunderstorm and Nosig days by using ERA5 dataset by examining the vertical profiles of temperature and relative humidity at each mandatory pressure levels in the troposphere.

Figure 2 shows the mean vertical profiles of temperature, wind, and relative humidity averaged on the thunderstorms and the Nosig days. The averaged temperature profiles do not clearly show a difference between the thunderstorm and Nosig days (Fig. 2a). However, Fig. 2b shows that the average relative humidity (RH) is generally higher on thunderstorm days than on Nosig days across all pressure levels, with the most pronounced differences observed in the middle layer (700–400 hPa). Previous studies showed that relative humidity is a key factor in characterizing tropical convective activity (Bourdin et al. 2021; Chakraborty et al. 2017; Kato 2006; Kikuchi and Takayabu 2004; Takemi et al. 2004; Kato 2006; Masunaga 2012; Romps 2014; Talev et al. 2008; Masunaga 2012; Romps 2014; Chakraborty et al. 2017; Bourdin et al. 2021). Thunderstorm days indicate a moist layer throughout the troposphere, including the middle

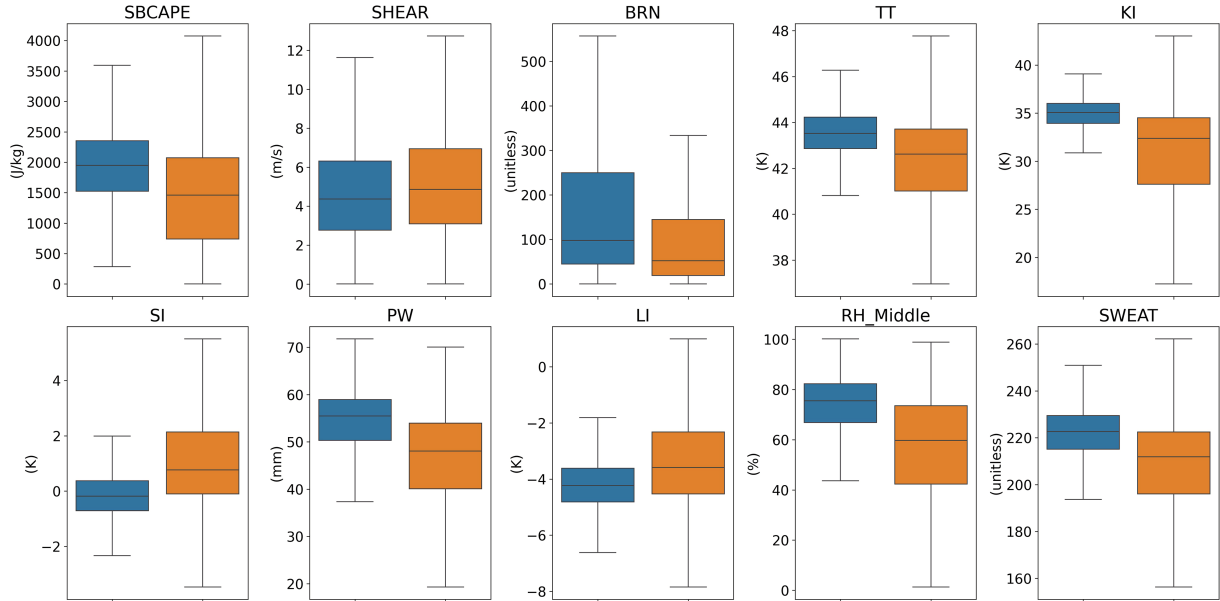


Fig. 3. The distribution of the stability indices listed in Table 1 as box-and-whisker plots under thunderstorm days (blue) and Nosig days (orange) conditions. The middle line of the box denotes the median value, the lower and upper edges of the box represent the first and third quartiles, and the upper and lower whiskers indicate the maximum and minimum values, respectively.

levels, while Nosig days demonstrate a drier layer between 700 and 400 hPa, with RH of about 25–60%. The analysis highlights the importance of RH in the middle troposphere as a key factor in distinguishing thunderstorm occurrences from Nosig weather in Indonesia, suggesting that the middle tropospheric RH affects convective processes across the region. Previous studies such as Takemi and Unuma (2019), Tsujino et al. (2021), Naka and Takemi (2023), and Jo and Lasher-Trapp (2023) also demonstrated that the middle tropospheric humidity strongly influences thunderstorm events, particularly in subtropical regions. This study extends those findings by demonstrating the effectiveness of RH in the middle layer for diagnosing thunderstorm events over the Maritime Continent, particularly Indonesia, further solidifying its relevance in tropical convective activity.

The vertical profile of average wind barbs (Fig. 2a) shows that the average wind speed below the 500-hPa level is weak under both thunderstorm and Nosig day conditions. At the upper levels above 500 hPa, winds are higher in the Nosig days than in the thunderstorm days, indicating that the vertical shear is stronger in the Nosig condition. Note here that the average wind barbs represent the average magnitudes of wind vectors, and the demonstrated calmness may partly result from high day-to-day variability rather than consistently weak winds.

3.2 Stability indices analysis

The stability indices listed in Table 1 are used to distinguish the environmental stability conditions between the thunderstorm and Nosig days. Figure 3 compares the frequency distributions of the indices under the thunderstorm and Nosig days. The distributions indicate that there are indices such as SBCAPE, SHEAR, and BRN that exhibit overlaps of the distributions between the thunderstorm and Nosig conditions, suggesting that the differences between the two conditions are less pronounced. The median value of SBCAPE on thunderstorm days is approximately 2000 J kg^{-1} , which is higher than the median value of 1500 J kg^{-1} on Nosig days. However, the range of SBCAPE values on Nosig days is broader, ranging from 0 to 4000 J kg^{-1} . The median SHEAR value on both thunderstorm and Nosig days is around 5 m s^{-1} , showing a minor difference. The median BRN value under thunderstorm days is around 100, which is due to the high SBCAPE values and weak shear, resulting in a higher BRN on thunderstorm days.

In contrast, other stability indices, TT, KI, SI, PW, LI, RH_Middle, and SWEAT, show a shift in distribution data between thunderstorm and Nosig days. These indices indicate less variance under thunderstorm days than under Nosig days. KI, PW, RH_Middle, and SWEAT typically show higher values on thunderstorm days than on Nosig days, reflecting the sensitivity of convective activity to middle-level RH. The distribution of lower SI also indicates increased instability on thunderstorm days.

3.3 Assessing thunderstorm potential environment days over Indonesia

To assess a potential environment for the development of thunderstorms, we examine the best normalized stability index to construct a logistic regression model as explained in Eq. (1). We aim to find an optimal probability threshold

Table 2. Logistic regression model for each stability index.

Index (x)	$P(x)$	Optimal probability thresholds	x
SBCAPE	$1 / (1 + \exp(-(-2.17 + 4.41 * x)))$	0.41	$(\ln[P(x)/1-P(x)] - (-2.17))/4.41$
TT	$1 / (1 + \exp(-(-1.88 + 2.75 * x)))$	0.44	$(\ln[P(x)/1-P(x)] - (-1.88))/2.75$
KI	$1 / (1 + \exp(-(-13.38 + 15.46 * x)))$	0.49	$(\ln[P(x)/1-P(x)] - (-13.38))/15.46$
SI	$1 / (1 + \exp(-(-1.66 + -6.14 * x)))$	0.45	$(\ln[P(x)/1-P(x)] - (-1.66))/-6.14$
PW	$1 / (1 + \exp(-(-6.88 + 10.16 * x)))$	0.48	$(\ln[P(x)/1-P(x)] - (-6.88))/10.16$
LI	$1 / (1 + \exp(-(-1.14 + -3.32 * x)))$	0.47	$(\ln[P(x)/1-P(x)] - (-1.14))/-3.32$
SHEAR	$1 / (1 + \exp(-(-0.28 + -1.06 * x)))$	0.50	$(\ln[P(x)/1-P(x)] - (-0.28))/-1.06$
BRN	$1 / (1 + \exp(-(-0.03 + 2.72 * x)))$	0.49	$(\ln[P(x)/1-P(x)] - (-0.03))/2.72$
RH_Middle	$1 / (1 + \exp(-(-3.82 + 5.77 * x)))$	0.44	$(\ln[P(x)/1-P(x)] - (-3.82))/5.77$
SWEAT	$1 / (1 + \exp(-(-5.35 + 7.23 * x)))$	0.48	$(\ln[P(x)/1-P(x)] - (-5.35))/7.23$

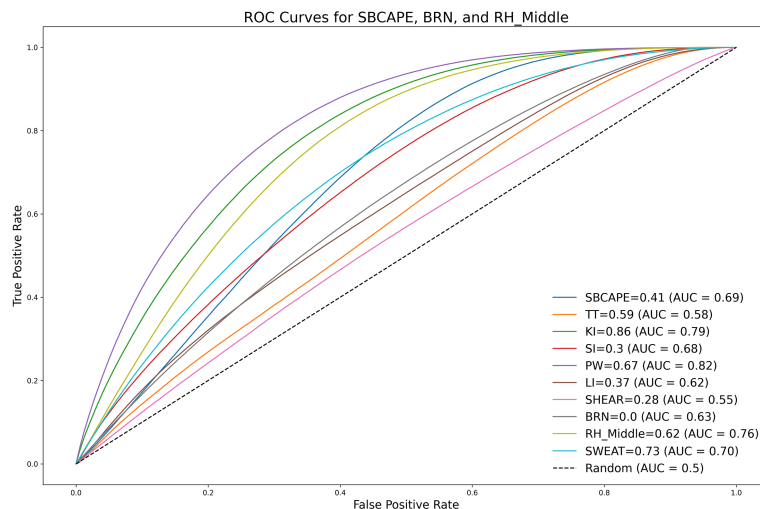


Fig. 4. The ROC curve for the stability indices obtained from the logistic regression model. The legend for each index includes the normalized values of the optimum thresholds and their AUC values.

with the highest AUC in the ROC analysis, and then convert it using Eq. (2) into the normalized threshold. Table 2 describes the logistic regression models for the environmental parameters and their optimal probability thresholds.

Figure 4 shows the ROC curves of the logistic regression model with different inputs of stability indices. The stability indices that have the three highest AUCs are PW, KI, and RH_Middle, with their AUC values being 0.82, 0.79, and 0.75, respectively. We use the normalized PW (0.67), KI (0.79), and RH_Middle (0.62) as optimal probability thresholds to map thunderstorm potential environments in Indonesia from 2014 to 2022. The mechanism for determining the optimal normalized threshold is detailed in Section 2.3. Thunderstorm potential environment days are defined as days where the values of PW, KI, and RH_Middle exceed their respective optimal normalized thresholds (0.67, 0.86, and 0.62). Figure 5a shows the average annual thunderstorm potential environment days, which can be compared with the average annual thunderstorm days derived from EGLN data (Fig. 5b). In general, the spatial patterns of the thunderstorm days are shown in Figs. 5a and 5b appear to be similar. This is evident from the similarity in areas with a high annual average frequency of thunderstorm days on both maps, such as the coastal areas of Sumatra near the Malacca Strait, West and Central Java, South Kalimantan, and Central Sulawesi. However, the average number of annual days that meet the thunderstorm potential environment criteria is higher than the actual average annual thunderstorm days. This discrepancy indicates a limitation in diagnosing a potential for thunderstorm development only from stability indices. Meeting the threshold for a thunderstorm potential environment does not guarantee the occurrence of thunderstorms owing to other factors such as storm initiation mechanisms and convective inhibition (Allen 2018). Additionally, there are limitations in ERA5 data in areas with little or no radiosonde data assimilated (Wu et al. 2024). Despite these overestimations and limitations, the diagnosis of the thunderstorm potential environment using the thresholds for stability indices is useful in capturing the spatial distribution pattern of thunderstorms.

Figures 5c and 5d show the performance of identifying thunderstorm potential days from the thresholds for PW, KI, and RH_Middle in terms of probability of detection (POD) and probability of false detection (POFD). Most areas have POD values above 0.7, indicating that thunderstorm days can be successfully predicted with the rate of greater

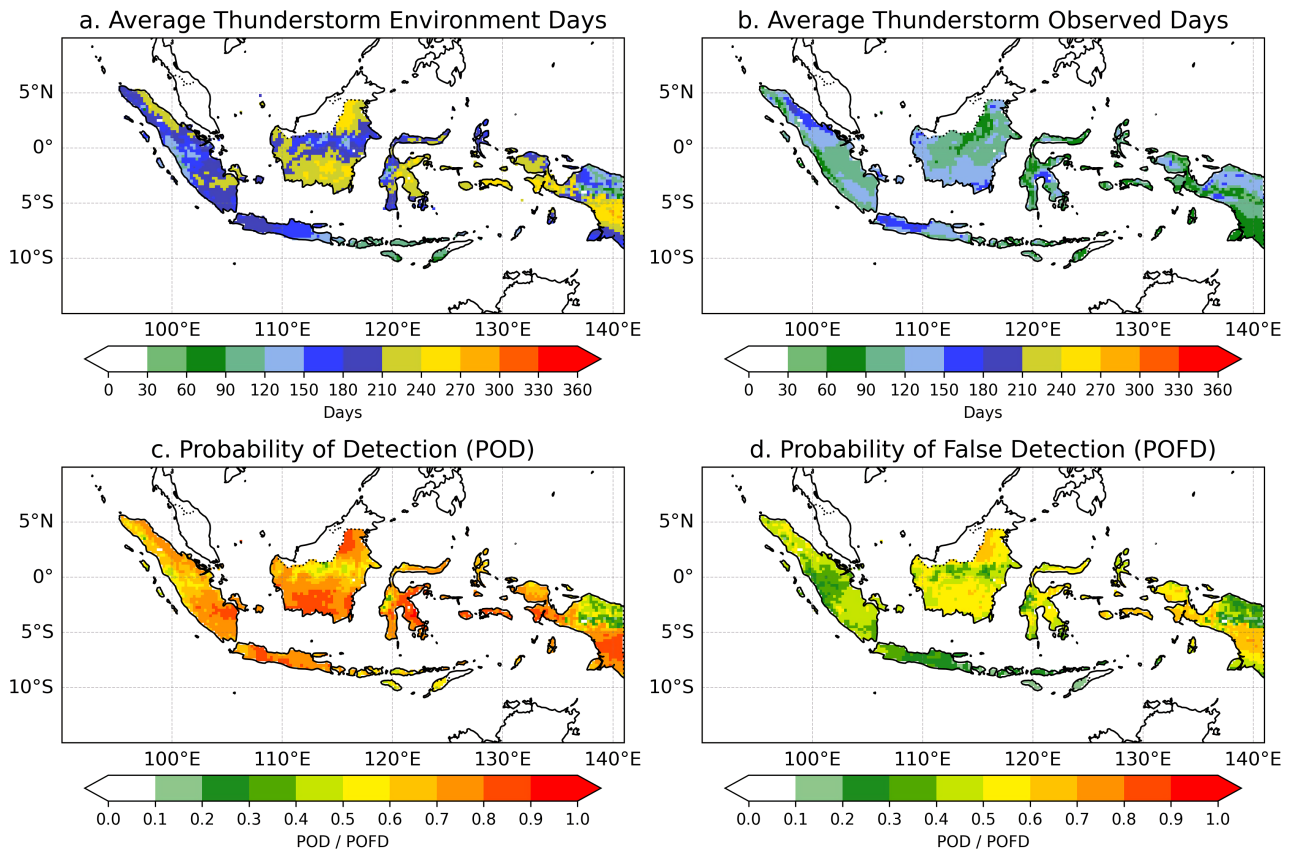


Fig. 5. The map of (a) the average annual number of days diagnosed as having thunderstorm potential environments, (b) the average annual number of observed thunderstorm days from the EGLN dataset, (c) the probability of detection (POD), and (d) the probability of false detection (POFD), calculated over the 9-year period (2014–2022).

than 70%. Conversely, most grids have POFD values between 0.3 and 0.4, indicating a detection error rate of 30–40% for thunderstorm days. Although most areas show favorable performance in identifying thunderstorm potential environment days, some regions with higher elevations, such as Central Kalimantan and mountainous areas in Papua, show poor performance. In these areas, in spite of fair performance of POD, POFD is also high, indicating that the index often exceeds the threshold even in the absence of thunderstorms. This suggests that, especially in areas with complex topography like Central Kalimantan and the mountains of Papua, the index may be less effective in predicting thunderstorms. This may be due to the low density of observation data, which affects the accuracy of ERA5 data in predicting thunderstorm events (Wu et al. 2024).

4. Discussion

In previous studies, CAPE and vertical wind shear generated from reanalysis datasets were successfully used as environmental proxies for favorable thunderstorm conditions in some mid-latitude regions (Romero et al. 2007; Brooks 2009; Haberlie et al. 2022; Allen et al. 2014; Pilguy et al. 2019; León-Cruz et al. 2023). However, in the present study, we found that the SBCAPE, a CAPE value calculated for a surface-based air parcel, performs unfavorably in distinguishing the conditions between thunderstorms and Nosig weather in Indonesia. A possible reason for such an unfavorable performance of SBCAPE in Indonesia is that Indonesia is a tropical maritime islands region where CAPE values are basically higher than in mid-latitude regions. In addition, the high SBCAPE values in the tropics indicate a high potential for the development of convective processes, but not all convective processes result in severe conditions (Doswell 1985). Therefore, under conditions with pronounced SBCAPE values, convective clouds will frequently grow, but sometimes without severe conditions. Another issue with using SBCAPE as a proxy for distinguishing thunderstorm conditions in Indonesia is the impact of large-scale phenomena like the Asian monsoon from November to March. During this period, the atmosphere tends to be more humid, and convective processes become more intense because of the increased middle-tropospheric moisture flux, which reduces the effectiveness of CAPE in predicting convective intensity (Jha et al. 2022; Jankov and Gallus 2003). The box-and-whisker plot analysis shows that the distributions of the SBCAPE values for the thunderstorm and Nosig conditions overlap. A similar distribution also occurs for vertical wind shear, which shows similar distributions between thunderstorm and Nosig conditions.

The similarity of the wind speed is considered to be attributable to the spatial resolution of the reanalysis data being about 25 km, which is not sufficient to explicitly resolve thunderstorm activity; alternatively, it might be attributable to the assumption that the dominant type of thunderstorms in Indonesia is a single-cell storm that develops in an environment with weak wind shear (Markowski and Richardson 2011). These results correspond to a statement by (Zinner and Groenemeijer 2012) that single-cell storms are more frequent in the tropics.

In this study, we found PW, KI, and RH_Middle to be the best stability indices with the AUC of greater than 0.75 in the ROC analysis to distinguish thunderstorm and Nosig conditions on the basis of the logistic regression method. The box-and-whisker plot analysis showed that the distributions of PW and KI under Nosig conditions indicate greater variances than those under thunderstorm conditions. The high values of PW resulted from both higher RH and a larger amount of water vapor content in the troposphere. Ng et al. (2022) showed that a high value of PW with weak vertical wind shear characterizes the environment for single-cell thunderstorms in southern China during summer (Ng et al. 2022). In addition, KI is useful in capturing thunderstorm conditions effectively because the KI formula takes into account the difference in temperature and dew point at the level of 700 hPa. The drier feature at the middle troposphere is found for the Nosig conditions, which reflects on the difference in KI between thunderstorm and Nosig conditions. This is consistent with the study of (Fernando et al. (2021) who demonstrated that KI more strongly affects thunderstorm events in the tropics than CAPE or CIN.

This study presents a new perspective on assessing thunderstorm conditions through the use of stability indices. The use of reanalysis data in this investigation provides benefits in terms of data accessibility and facilitates a comprehensive climatological examination. However, increasing the density of upper-air observation data and improving the vertical resolution of reanalysis data are still necessary to enhance the accuracy of vertical temperature profile estimations (Allen et al. 2014; Wang et al. 2020), which may affect the calculation of stability indices for predicting thunderstorm conditions in areas with complex topography. The results of this study encourage further exploration of the factors controlling deep convection over the complex topographies across Indonesia (Teo et al. 2011; Wu et al. 2009). Additionally, future studies could explore the application of more advanced models, such as multiple logistic regression, to identify combinations of indices and their thresholds for determining thunderstorm potential environment days.

5. Conclusion

This study investigates, by using ERA5 data, the environmental properties of thunderstorm activity and the difference in the environment between the thunderstorm and no significant weather (Nosig) days. The vertical distribution of temperature does not exhibit a distinct variation between days characterized by thunderstorms and those classified as Nosig; however, the relative humidity (RH) within the middle troposphere reveals a significant difference between the two conditions. Under Nosig conditions, the middle troposphere displays RH values ranging from approximately 25% to 65%, while during thunderstorm conditions, the middle tropospheric RH values are observed to be between about 60% and 80%. Overall, atmospheric stability indices do not fully differentiate between thunderstorm and Nosig conditions, as certain values are present in both conditions, as illustrated by the box-and-whisker plot analyses.

By applying a logistic regression approach, we find that PW, KI and RH_Middle are the three most effective parameters in distinguishing between thunderstorm and Nosig conditions using normalized threshold values of 0.67, 0.86, and 0.62, respectively. This analysis was used to map the thunderstorm potential areas in Indonesia.

This approach provides a feasible method to identify the different potential risks of thunderstorms in different regions in Indonesia. Using a statistics method, the proposed method offers unprecedented insight into finding effective stability indices to distinguish thunderstorms and Nosig conditions in Indonesia. In a future work, we plan to explore the variability of thunderstorm potential environment based on atmospheric stability index to other global scale phenomena in Indonesia.

Acknowledgments

The authors would like to thank the editor and anonymous reviewers for their helpful comments and suggestions. Thunder hour dataset downloaded from <http://thunderhours.earthnetworks.com/>. The CHIRPS dataset downloaded from <https://data.chc.ucsb.edu/products/CHIRPS-2.0/>. ERA5 data (Hersbach et al. 2020) from the European Centre for Medium-Range Weather Forecasts was downloaded at <https://cds.climate.copernicus.eu/cdsapp#!/dataset/reanalysis-era5-pressure-levels?tab=form>. This work was supported by PhD grant of Indonesia Endowment Fund for Education (LPDP), the Japan Society for the Promotion of Science (JSPS) Scientific Research 20H00289 and 24H00369 and also by the advanced studies of climate change projection (SENTAN) Grant Number JPMXD0722678534 from the Ministry of Education, Culture, Sports, Science and Technology (MEXT) of Japan.

Supplements

A detailed explanation of how to find the optimal stability indices and determine the optimal normalized threshold for each index.

References

- Allen, J. T., 2018: Climate change and severe thunderstorms. *Oxford Research Encyclopedia of Climate Science*, doi:10.1093/acrefore/9780190228620.013.62.
- Allen, J. T., D. J. Karoly, and G. A. Mills, 2011: A severe thunderstorm climatology for Australia and associated thunderstorm environments. *Aust. Meteor. Oceanogr. J.*, **61**, 143–158, doi:10.22499/2.6103.001.
- Allen, J. T., D. J. Karoly, and K. J. Walsh, 2014: Future Australian severe thunderstorm environments. Part I: A novel evaluation and climatology of convective parameters from two climate models for the late twentieth century. *J. Climate*, **27**, 3827–3847, doi:10.1175/JCLI-D-13-00425.1.
- Bachok, M. F., S. Shamsudin, and R. Z. Abidin, 2015: Effectiveness of windstorm-producing thunderstorms early warning issues in peninsular Malaysia. *Int. J. Environ. Sci. Dev.*, **6**, 635–642, doi:10.7763/IJESD.2015.V6.672.
- Bondyopadhyay, S., and M. Mohapatra, 2023: Determination of suitable thermodynamic indices and prediction of thunderstorm events for Eastern India. *Meteor. Atmos. Phys.*, **135**, 4, doi:10.1007/s00703-022-00942-1.
- Bourdin, S., L. Kluft, and B. Stevens, 2021: Dependence of climate sensitivity on the given distribution of relative humidity. *Geophys. Res. Lett.*, **48**, e2021GL092462, doi:10.1029/2021GL092462.
- Brooks, H. E., 2009: Proximity soundings for severe convection for Europe and the United States from reanalysis data. *Atmos. Res.*, **93**, 546–553, doi:10.1016/j.atmosres.2008.10.005.
- Brooks, H. E., J. W. Lee, and J. P. Craven, 2003: The spatial distribution of severe thunderstorm and tornado environments from global reanalysis data. *Atmos. Res.*, **67–68**, 73–94, doi:10.1016/S0169-8095(03)00045-0.
- Chakraborty, R., S. Talukdar, U. Saha, S. Jana, and A. Maitra, 2017: Anomalies in relative humidity profile in the boundary layer during convective rain. *Atmos. Res.*, **191**, 74–83, doi:10.1016/J.ATMOSRES.2017.03.011.
- Davies-Jones, R., 2015: A review of supercell and tornado dynamics. *Atmos Res.*, **158–159**, 274–291, doi:10.1016/J.ATMOSRES.2014.04.007.
- Davies-Jones, R., 2022: Theory of parcel vorticity evolution in supercell-like flows. *J. Atmos. Sci.*, **79**, 1253–1270, doi:10.1175/JAS-D-21-0178.1.
- Dhamira, A., and I. Irham, 2020: The impact of climatic factors on rice production in Indonesia. *Agro Ekonomi*, **31**, 46–60, doi:10.22146/ae.55153.
- DiGangi, E. A., M. Stock, and J. Lapierre, 2022: Thunder hours: How old methods offer new insights into thunderstorm climatology. *Bull. Amer. Meteor. Soc.*, **103**, E549–E569, doi:10.1175/BAMS-D-20-0198.1.
- Estiningtyas, W., H. Syahbuddin, Harmanto, A. Pramudia, and S. K. Dermoredjo, 2021: Analysis of key locations as indicators for extreme climate impacts in supporting climate change adaptation in Indonesia. *IOP Conf. Ser. Earth Environ. Sci.*, **724**, 012042, doi:10.1088/1755-1315/724/1/012042.
- Fernando, M., M. Millangoda, and S. Premalal, 2021: Analyze and comparison of the atmospheric instability using K-Index, Lifted Index Total Totals Index Convective Availability Potential Energy (CAPE) and Convective Inhibition (CIN) in development of thunderstorms in Sri Lanka during second inter-monsoon. *Multi-Hazard Early Warning and Disaster Risks*. D. Amaratunga, R. Haigh, and N. Dias, Eds., Springer International Publishing, 603–614.
- Funk, C., and co-authors, 2015: The climate hazards infrared precipitation with stations—a new environmental record for monitoring extremes. *Sci. Data*, **2**, 150066, doi:10.1038/sdata.2015.66.
- Galway, J. G., 1956: The lifted index as a predictor of latent instability. *Bull. Amer. Meteor. Soc.*, **37**, 528–529, doi:10.1175/1520-0477-37.10.528.
- George, J. J., 1960: *Weather Forecasting for Aeronautics*. Academic Press, 673 pp.
- Haberlie, A. M., W. S. Ashley, C. M. Battisto, and V. A. Gensini, 2022: Thunderstorm activity under intermediate and extreme climate change scenarios. *Geophys. Res. Lett.*, **49**, e2022GL098779, doi:10.1029/2022GL098779.
- Hamid, E. Y., Z.-I. Kawasaki, and R. Mardiana, 2001: Impact of the 1997–98 El Niño event on lightning activity over Indonesia. *Geophys. Res. Lett.*, **28**, 147–150, doi:10.1029/2000GL011374.
- Hanstrum, B. N., G. A. Mills, A. Watson, J. P. Monteverdi, and C. A. Doswell III, 2002: The cool-season tornadoes of California and southern Australia. *Wea. Forecasting*, **17**, 705–722, doi:10.1175/1520-0434(2002)017<0705:TCSTOC>2.0.CO;2.
- Hersbach, H., and co-authors, 2020: The ERA5 global reanalysis. *Quart. J. Roy. Meteor. Soc.*, **146**, 1999–2049, doi:10.1002/QJ.3803.
- Hidayat, S., and M. Ishii, 1999: Diurnal variation of lightning characteristics around Java Island. *J. Geophys. Res.*, **104**, 24449–24454, doi:10.1029/1999JD900769.

- Hobbs, P. V., and J. M. Wallace, 2006: *Atmospheric Science: An Introductory Survey. Second Edition*. Academic Press, 504 pp.
- Jankov, I., and W. A. Gallus Jr., 2004: MCS rainfall forecast accuracy as a function of large-scale forcing. *Wea. Forecasting*, **19**, 428–439.
- Jha, A. K., S. K. Das, S. M. Deshpande, and U. V. Murali Krishna, 2022: Understanding the relationship of storm- to large-scale environment in the monsoon trough region: Results inferred from long-term radar and reanalysis datasets. *Quart. J. Roy. Meteor. Soc.*, **148**, 97–116, doi:10.1002/qj.4194.
- Jo, E., and S. Lasher-Trapp, 2023: Entrainment in a simulated supercell thunderstorm. Part III: The influence of decreased environmental humidity and general effects upon precipitation efficiency. *J. Atmos. Sci.*, **80**, 1107–1122, doi:10.1175/JAS-D-22-0168.1.
- Kato, T., 2006: Structure of the band-shaped precipitation system inducing the heavy rainfall observed over northern Kyushu, Japan on 29 June 1999. *J. Meteor. Soc. Japan*, **84**, 129–153, doi:10.2151/jmsj.84.129.
- Kikuchi, K., and Y. N. Takayabu, 2004: The development of organized convection associated with the MJO during TOGA COARE IOP: Trimodal characteristics. *Geophys. Res. Lett.*, **31**, L10101, doi:10.1029/2004GL019601.
- León-Cruz, J. F., E. Caetano, J. Cortés-Ramos, C. Dominguez, and J. M. Méndez-Pérez, 2023: Thunderstorm and hailstorm environments in Mexico. *Int. J. Climatol.*, **43**, 4379–4395, doi:10.1002/joc.8093.
- Markowski, P., and Y. Richardson, 2011: *Mesoscale Meteorology in Midlatitudes*. John Wiley & Sons, 407 pp.
- Masunaga, H., 2012: Short-term versus climatological relationship between precipitation and tropospheric humidity. *J. Climate*, **25**, 7983–7990, doi:10.1175/JCLI-D-12-00037.1.
- May, R. M., and co-authors, 2022: MetPy: A meteorological python library for data analysis and visualization. *Bull. Amer. Meteor. Soc.*, **103**, E2273–E2284, doi:10.1175/BAMS-D-21-0125.1.
- Miller, R. C., 1975: *Notes on Analysis and Severe-storm Forecasting Procedures of the Air Force Global Weather Central*. Air Weather Services (MAC), United States Air Force.
- Naka, N., and T. Takemi, 2023: Characteristics of the environmental conditions for the occurrence of recent extreme rainfall events in Northern Kyushu, Japan. *SOLA*, **19A**, 9–16, doi:10.2151/SOLA.19A-002.
- Ng, C.-P., Q. Zhang, W. Li, and Z. Zhou, 2022: Contribution of thunderstorms to changes in hourly extreme precipitation over China from 1980 to 2011. *J. Climate*, **35**, 4485–4498, doi:10.1175/JCLI-D-21-0701.1.
- Pang, G., J. He, Y. Huang, and L. Zhang, 2019: A binary logistic regression model for severe convective weather with numerical model data. *Adv. Meteor.*, **2019**, 6127281, doi:10.1155/2019/6127281.
- Pilgus, N., M. Taszarek, Ł. Pajurek, and M. Kryza, 2019: High-resolution simulation of an isolated tornadic supercell in Poland on 20 June 2016. *Atmos. Res.*, **218**, 145–159, doi:10.1016/j.atmosres.2018.11.017.
- Pradhan, D., U. K. De, and U. V. Singh, 2012: Development of nowcasting technique and evaluation of convective indices for thunderstorm prediction in Gangetic West Bengal (India) using Doppler Weather Radar and upper air data. *MAUSAM*, **63**, 299–318, doi:10.54302/mausam.v63i2.1427.
- Ramage, C. S., 1968: Role of a tropical “maritime continent” in the atmospheric circulation. *Mon. Wea. Rev.*, **96**, 365–370.
- Romero, R., M. Gayà, and C. A. Doswell III, 2007: European climatology of severe convective storm environmental parameters: A test for significant tornado events. *Atmos. Res.*, **83**, 389–404, doi:10.1016/j.atmosres.2005.06.011.
- Romps, D. M., 2014: An analytical model for tropical relative humidity. *J. Climate*, **27**, 7432–7449, doi:10.1175/JCLI-D-14-00255.1.
- Salby, M. L., 1996: *Fundamentals of Atmospheric Physics*. Academic Press, 627 pp.
- Sherburn, K. D., 2018: Environments and origins of low-level vortices within high-shear, low-CAPE convection. Dissertation, North Carolina State University (Available online at <https://search.proquest.com/openview/bad6f97f2ff9a0e6966a6ef52f2a51d7/1?pq-origsite=gscholar&cbl=18750>, accessed 2 July 2024).
- Showalter, A. K., 1953: A stability index for thunderstorm forecasting. *Bull. Amer. Meteor. Soc.*, **34**, 250–252.
- Singh, M. S., Z. Kuang, E. D. Maloney, W. M. Hannah, and B. O. Wolding, 2017: Increasing potential for intense tropical and subtropical thunderstorms under global warming. *Proc. Natl. Acad. Sci. U.S.A. (PNAS)*, **114**, 11657–11662, doi:10.1073/pnas.1707603114.
- Subasi, A., 2020: *Practical Machine Learning for Data Analysis Using Python*. Elsevier, 1–520.
- Swets, J. A., 1988: Measuring the accuracy of diagnostic systems. *Science*, **240**, 1285–1293, doi:10.1126/science.3287615.
- Takemi, T., 2010: Dependence of the precipitation intensity in mesoscale convective systems to temperature lapse rate. *Atmos. Res.*, **96**, 273–285, doi:10.1016/j.atmosres.2009.09.002.
- Takemi, T., and T. Unuma, 2019: Diagnosing environmental properties of the July 2018 heavy rainfall event in Japan. *SOLA*, **15A**, 60–65, doi:10.2151/sola.15a-011.
- Takemi, T., O. Hirayama, and C. Liu, 2004: Factors responsible for the vertical development of tropical oceanic cumu-

- lus convection. *Geophys. Res. Lett.*, **31**, L11109, doi:10.1029/2004GL020225.
- Talev, G., A. Gustavsen, and E. Næss, 2008: Influence of the velocity, local position, and relative humidity of moist air on the convective mass transfer coefficient in a rectangular tunnel—theory and experiments. *J. Build. Phys.*, **32**, 155–173, doi:10.1177/1744259108091564.
- Taszarek, M., J. T. Allen, H. E. Brooks, N. Pilguy, and B. Czernecki, 2021: Differing trends in United States and European severe thunderstorm environments in a warming climate. *Bull. Amer. Meteor. Soc.*, **102**, E296–E322, doi:10.1175/BAMS-D-20-0004.1.
- Teo, C.-K., T.-Y. Koh, J. C.-F. Lo, and B. C. Bhatt, 2011: Principal component analysis of observed and modeled diurnal rainfall in the Maritime Continent. *J. Climate*, **24**, 4662–4675, doi:10.1175/2011JCLI4047.1.
- Tian, F., X. Zhang, J. Sun, K. Xia, S. Hua, Q. Wei, L. Xue, and B. Yang, 2023: Climatology and pre-convection environmental conditions of dry and wet thunderstorm high winds over eastern China. *Theor. Appl. Climatol.*, **155**, 1493c1506, doi:10.1007/s00704-023-04704-w.
- Tsujino, S., H.-C. Kuo, H. Yu, B.-F. Chen, and K. Tsuboki, 2021: Effects of mid-level moisture and environmental flow on the development of afternoon thunderstorms in Taipei. *Terr. Atmos. Oceanic Sci.*, **32**, 497–518, doi:10.3319/TAO.2021.11.17.01.
- Virts, K. S., J. M. Wallace, M. L. Hutchins, and R. H. Holzworth, 2013: Highlights of a new ground-based, hourly global lightning climatology. *Bull. Amer. Meteor. Soc.*, **94**, 1381–1391, doi:10.1175/BAMS-D-12-00082.1.
- Viteri López, A. S., and C. A. Morales Rodriguez, 2020: Flash flood forecasting in São Paulo using a binary logistic regression model. *Atmosphere*, **11**, 473, doi:10.3390/atmos11050473.
- Wang, Z., J. A. Franke, Z. Luo, and E. J. Moyer, 2021: Reanalyses and a high-resolution model fail to capture the “high tail” of CAPE distributions. *J. Climate*, **34**, 8699–8715, doi:10.1175/JCLI-D-20-0278.1.
- Wu, J., and co-authors, 2024: Can ERA5 reanalysis data characterize the pre-storm environment? *Atmos. Res.*, **297**, 107108, doi:10.1016/j.atmosres.2023.107108.
- Wu, P., J.-I. Hamada, M. D. Yamanaka, J. Matsumoto, and M. Hara, 2009: The impact of orographically-induced gravity waves on the diurnal cycle of rainfall over southeast Kalimantan Island. *Atmos. Oceanic Sci. Lett.*, **2**, 35–39, doi:10.1080/16742834.2009.11446773.
- Yuan, T., Y. Di, and K. Qie, 2016: Variability of lightning flash and thunderstorm over East/Southeast Asia on the ENSO time scales. *Atmos. Res.*, **169**, 377–390, doi:10.1016/j.atmosres.2015.10.022.
- Zinner, T., and P. Groenemeijer, 2012: Thunderstorms: Thermodynamics and organization. *Atmospheric Physics: Background–Methods–Trends*. 1st ed. U. Schumann, Ed., Springer, 101–114.
- Zipser, E. J., 1994: Deep cumulonimbus cloud systems in the tropics with and without lightning. *Mon. Wea. Rev.*, **122**, 1837–1851, doi:10.1175/1520-0493(1994)122<1837:DCCSIT>2.0.CO;2.